

Overturning and wind driven circulation in a low-order ocean-atmosphere model

Submitted to *Dyn. Atmos. Oceans*.

ABSTRACT. A low-order ocean-atmosphere model is presented which combines coupling through heat exchange at the interface and wind stress forcing. The coupling terms are derived from the boundary conditions and the forcing terms of the constituents. Both the ocean and the atmosphere model are based on Galerkin truncations of the basic fluid dynamical equations. Hence, the coupled model can readily be extended to include more physics and more detail. The model presented here is the simplest of a hierarchy of low-order ocean-atmosphere models. The behaviour of the coupled model is investigated by means of geometric singular perturbation theory and bifurcation analysis. Two ways are found in which the slow time scales can play a role in the coupled dynamics. In the first scenario, a limit cycle on the overturning time scale is created. The associated oscillatory behaviour is governed by internal ocean dynamics. In the second scenario intermittent behaviour occurs between periodic and chaotic regimes in parameter space.

1. Introduction

Until recently, the study of ocean models of low order has been restricted to a rather conceptual level. A variety of models have been constructed using the idea of Stommel [1961], dividing the ocean, or rather a meridional plane, into compartments. Within each compartment, the temperature and salinity of the sea water are constant and the flux of these quantities is based on diffusion-like dynamics. Such models are used to investigate the stability of the overturning circulation. Coexisting equilibria then represent different orientations of the overturning. Extensions of Stommel's model have been constructed to allow for oscillatory behaviour [Welander, 1982; Titz et al., 2002] and to mimic wind driven circulation [Huang and Stommel, 1992]. Low-order climate models usually rely on Stommel type ocean models, such as in Nakamura et al. [1994]; Roebber [1995]; van Veen et al. [2001]. Distinct disadvantages of such models are that they cannot be derived from the physical equations by means of Galerkin truncation and they cannot include rotation.

The wind driven circulation has also been investigated by means of low-order models. Veronis [1963], for instance, studied multiple equilibria and oscillatory behaviour in a model with four degrees of freedom. His findings were validated by comparison to a model of intermediate complexity [Jerley and Sheremet, 1995]. In

that work the two dimensional Navier-Stokes equations govern the flow. Consequently the overturning circulation is absent.

The Maas [1994] model, in contrast, allows for the study of both overturning and wind driven circulation in a low-order setting. Also, its formulation in terms of a Galerkin truncation of the angular momentum and density fields links it directly to the governing fluid dynamical equations.

We couple the angular momentum based ocean model to the Lorenz-84 model for the atmosphere. As shown in van Veen [2002], the latter model approximates the dynamics of a baroclinic atmosphere model. The physical processes thus represented in the coupled model are thermally induced overturning, wind driven gyre circulation and, in the atmosphere, baroclinic wave activity.

The aim of this paper is twofold: firstly to describe the scaling and the coupling of the model in some detail and secondly to explore the dynamics of the coupled system by means of perturbation theory and bifurcation analysis.

In section (2) the ocean-atmosphere interaction terms are calculated from the surface integrals which appear in the ocean's boundary conditions and the atmosphere's forcing terms. The difference in time scales between the wind driven, the overturning and the atmospheric dynamics, as well as the coupling strengths, follow from the physically relevant scaling. The coupled model, presented here, is in a sense the simplest of a family of low-order ocean-atmosphere models. In the concluding section a number of possible extensions is listed.

In section (3), we explore the behaviour of the model by means of Fenichel theory, or, more specifically, Geometric Singular Perturbation (GSP) theory. A bifurcation analysis is conducted in section (4). In this analysis, the focus is on the question how the slow dynamics of the ocean model can show up in the dynamics of the coupled model.

GSP theory is applied in the regime where the atmosphere is in an equilibrium state. In this case, no instabilities are excited in the ocean model, except when the atmosphere's equilibrium is nearly critical. In that case, a Hopf bifurcation can occur which produces a weakly unstable cycle on the overturning time scale. The occurrence of this Hopf bifurcation is connected to the presence of a Bogdanov-Takens point at nearby parameter values. The unfolding of this point and the consequences for the coupled dynamics are discussed in section (4.1). The oscillatory behaviour induced by the cycle is generated by internal ocean dynamics.

A window in parameter space is shown to exist where the behaviour is chaotic, with tiny periodic intervals. In the fully chaotic regime the climatology of the model is studied. The physical processes represented in the model are simulated to reasonable accuracy. Near the boundary of stable periodic motion, intermittency can occur. Here, the slow subsystem, i.e. the ocean, can cause the fast subsystem, i.e. the atmosphere, to pass through a sequence of bifurcations repeatedly. This phenomenon was already observed in the Lorenz-Stommel model [van Veen, 2002]. Thus, the slow time scale shows up in the transition time between regimes of qualitatively different behaviour. This is a second way for the slow dynamics to influence the behaviour of the coupled system.

To the author's knowledge, no low-order ocean-atmosphere model which combines wind driven and overturning circulation has been studied before. The model analysis presented here is far from exhaustive. The presence of small parameters in the model suggests the use of perturbation theory, also in the regime where the atmosphere is not in equilibrium. Such a perturbation theory involves averaging over the fast time scale [Rödenbeck et al., 2001]. In future research, this technique will be applied to the Lorenz-Maas model [Arnold and Olbers, 2002]. Also, the coupled system might be compared to the Maas model with stochastic forcing [Monahan, 2001]. The computation of Lyapunov exponents and attractor dimensions might reveal to what extent chaotic, deterministic forcing is different from forcing by noise.

2. Description of the model

The ocean model was formulated in Maas [1994, 2002]. The atmosphere model is due to Lorenz [1984] and was provided with a physical basis in van Veen [2002]. Here, we will show how the coupling terms and multiple time scales are introduced.

2.1. Scaling of the low order models. The ocean model is valid in a rectangular domain with width and length L and height H . This basin is assumed to have a rigid lid. We choose Cartesian coordinates about the basin's geometric centre. The fluid motion is governed by the Navier-Stokes equations in the Boussinesq approximation on an f -plane. It is described by the basin averaged angular momentum and the linear variations of the density field, ρ , defined respectively as

$$\mathbf{L} = \frac{1}{V} \int \mathbf{x} \times \mathbf{u} dV \quad \rho_x = \frac{\int x \rho dV}{\int x^2 dV} \quad \rho_y = \frac{\int y \rho dV}{\int y^2 dV} \quad \rho_z = \frac{\int z \rho dV}{\int z^2 dV} \quad (1)$$

Here $V = L^2 H$ is the volume of the domain, \mathbf{u} is the velocity of the fluid and the density field is defined as $\rho = (\rho_* - \rho_0) / \delta\rho$, i.e. the difference between the dimensional field, ρ_* and a constant reference field, ρ_0 , scaled by a typical fluctuation, $\delta\rho$. The salinity of the ocean is not taken into account, so that the density is determined by the temperature alone. We define the non-dimensional temperature by $T = \alpha(T_* - T_0) / \delta\rho$, where α is the thermal expansion coefficient. Thus, we have

$$\rho = x\rho_x + y\rho_y + z\rho_z \quad \text{and} \quad T = -\rho. \quad (2)$$

In this approximation the model has six degrees of freedom. In a scaling appropriate for overturning dynamics, however, we see that the inertia of the horizontal angular momentum can be neglected.

The dynamical equations for \mathbf{L} and $\rho_{x,y,z}$ are

$$\frac{d}{dt}\mathbf{L} = -\frac{f}{2}\mathbf{k} \times \mathbf{L} + \frac{H^2 g \delta \rho}{12 \rho_0} (-\rho_y \mathbf{i} + \rho_x \mathbf{j}) - (r_h L_1, r_h L_2, r_v L_3)^T + \mathbf{T} \quad (3.1)$$

$$\frac{L^2}{12} \frac{d}{dt} \rho_x = -\frac{1}{2} L_3 \rho_y + \frac{1}{2} L_2 \rho_z - K_h \rho_x + F^{(x)} \quad (3.2)$$

$$\frac{L^2}{12} \frac{d}{dt} \rho_y = -\frac{1}{2} L_1 \rho_z + \frac{1}{2} L_3 \rho_x - K_h \rho_y + F^{(y)} \quad (3.3)$$

$$\frac{H^2}{12} \frac{d}{dt} \rho_z = -\frac{1}{2} L_2 \rho_x + \frac{1}{2} L_1 \rho_y - K_v \rho_z + F^{(z)} \quad (3.4)$$

where $\mathbf{i}, \mathbf{j}, \mathbf{k}$ are the unit vectors in the x, y and z direction, f is the Coriolis parameter, g is the acceleration of gravity, r_h and r_v are the horizontal and vertical Rayleigh damping coefficients and K_h and K_v are the horizontal and vertical eddy diffusivity constants. The forcing terms \mathbf{T} and \mathbf{F} stand for the wind stress torque and the buoyancy flux at the surface. In the following we will assume that $F^{(x)} = F^{(z)} = 0$ and $T_1 = T_2 = 0$. The remaining forcing terms, $F^{(y)}$ and T_3 represent meridional differential heating and wind shear forcing, respectively.

The Cartesian coordinates will be scaled as $[x, y, z] = [L, L, H]$, and the density fluctuations as $[\delta \rho] = [12 \rho_0 r_h K_h / g H]$. The time scale of interest is different for the overturning, the wind driven and the atmospheric dynamics in the coupled model. As described below, this difference of time scales leads to the introduction of a small parameter in the model.

A typical time scale for the overturning dynamics, described by the horizontal components of the angular momentum, $L_{1,2}$, is given by $\Sigma_1^{-1} = L^2 / K_h$. Let $t_1 = \Sigma_1 t$ and let primes denote non-dimensional quantities, then we find from equation (3.1) that

$$\begin{aligned} \frac{1}{Pr} \frac{d}{dt_1} L'_1 &= f' L'_2 - \delta \rho' \rho'_y - L'_1 \\ \frac{1}{Pr} \frac{d}{dt_1} L'_2 &= -f' L'_1 + \delta \rho' \rho'_x - L'_2 \end{aligned} \quad (4)$$

where $f' = f/2r_h$ is the scaled Coriolis parameter and $Pr = r_h L^2 / K_h$ is the Prandtl number. A realistic value of Pr is $O(10^5)$. Therefore, we consider the limit $Pr \rightarrow \infty$, obtaining

$$\begin{pmatrix} L'_1 \\ L'_2 \end{pmatrix} = \frac{\delta \rho'}{1 + f'^2} \begin{pmatrix} f' & -1 \\ 1 & f' \end{pmatrix} \begin{pmatrix} \rho'_x \\ \rho'_y \end{pmatrix} \quad (5)$$

The vertical component of the angular momentum is driven by wind shear forcing. Therefore, we introduce a second time scale, reasonable for the ocean's boundary layer. It is given by $\Sigma_2^{-1} = r_v^{-1}$. With $L'_3 = L_3 / L^2 \Sigma_1$ and $t_2 = \Sigma_2 t$ we have

$$\frac{d}{dt_2} L'_3 = -L'_3 + T'_3 \quad (6)$$

where $T'_3 = T_3 / L^2 \Sigma_1 \Sigma_2$ is the dimensionless torque due to wind stress. Note, that we have scaled L_3 by a factor Σ_1 and its tendency by a factor Σ_2 . This hybrid formulation is necessary to make up for the absence of an explicit boundary layer

in the model. The wind shear directly drives the basin averaged vertical angular momentum. In reality, the influence of the wind stress is manifest in a boundary layer of thickness h , and rapidly decreases below that. Therefore, we will include a factor of h/H in the forcing strength, as discussed below.

In order to get rid of the numerical factors in equations (3.2-4) we rescale t_1 by a factor $1/12$, \mathbf{u} by a factor 2 and set $\delta\rho' = 2$. Then, using relation (5) to eliminate $L_{1,2}$, we obtain

$$\frac{d}{dt_1}\rho'_x = -\rho'_y L'_3 + \frac{1}{1+f'^2}(\rho'_x + f'\rho'_y)\rho'_z - \rho'_x \quad (7.1)$$

$$\frac{d}{dt_1}\rho'_y = \rho'_x L'_3 - \frac{1}{1+f'^2}(f'\rho'_x - \rho'_y)\rho'_z - \rho'_y + F^{(y)'} \quad (7.2)$$

$$\frac{d}{dt_1}\rho'_z = -\rho'^2_x - \rho'^2_y - \mu\rho'_z \quad (7.3)$$

Where $\mu = K_v L^2 / K_h H^2$. The set of equations (6) and (7) forms the ocean model. It will be coupled to the atmosphere model through the wind stress torque, T_3 and the differential heating term $F^{(y)'}$. The coupling will be discussed in section (2.2)

The horizontal spatial scale of the atmosphere model is identical to that of the ocean model. The time scale of the Lorenz-84 model is set to Σ_3^{-1} , the damping time scale of baroclinic waves. The model's equations are

$$\dot{X} = -Y^2 - Z^2 - aX + aF \quad (8.1)$$

$$\dot{Y} = XY - bXZ - Y + G \quad (8.2)$$

$$\dot{Z} = bXY + XZ - Z \quad (8.3)$$

where F stands for forcing by differential heating in the meridional direction and G in the zonal direction, e.g. through land-sea contrast. The damping time scale of the zonally symmetric westerlies with respect to that of the baroclinic waves is set by a while b determines the strength of passive advection relative to the exchange of energy between the baroclinic waves and the westerlies, i.e. the jet stream.

As shown in van Veen [2002], equations (8.1-3) approximate the dynamics of a severe truncation of a quasi-geostrophic two layer model on an f -plane. The mean and shear streamfunctions, Ψ and τ , consist of a zonally symmetric part, representing the jet stream, and a sinusoidal wave. They are related to X , Y and Z through

$$\Psi' = -X \sin \pi y' + \sqrt{2} \cos \pi y' (Y \sin \pi x' + Z \cos \pi x') \quad (9.1)$$

$$\tau' = -X \sin \pi y' + \sqrt{2} \cos \pi y' (Z \sin \pi x' - Y \cos \pi x') \quad (9.2)$$

with Ψ' and τ' in units $[L^2 \Sigma_3]$ and $(x', y') \in [-1, 1] \times [-1/2, 1/2]$. The jet stream pattern is equivalent barotropic whereas the wave is optimally baroclinic. The mean potential temperature, Θ , can be calculated from the shear stream function using the thermal wind relation. Let $\Theta = \Theta_{av} + \theta$, where Θ_{av} is the average potential temperature over the whole domain, and θ is the local departure. Then we have

$$\theta' = \tau' \quad (10)$$

with θ' in units $[\Theta] = [f\Sigma_3 L^2 / dc_p^a]$. Here, c_p^a is the specific heat of dry air at constant pressure and the non-dimensional constant $d = 0.124$ results from the vertical discretisation. The vertical gradient of potential temperature, σ , is kept constant. The feedback to the atmosphere will be represented by a modulation of the meridional heating gradient, induced by heat exchange at the ocean's surface.

2.2. Coupling terms. We consider two kinds of interaction between ocean and atmosphere: wind driven circulation and heat flux at the ocean's surface. The former interaction is represented by the forcing term T_3 in equation (6) for the evolution of the vertical angular momentum. The latter is represented by a modification of the forcing terms representing differential heating in the meridional direction, $F^{(y)}$ in equation (7.2) and F in equation (8.1). The effect of baroclinic waves in the atmosphere on the wind driven circulation is excluded, and so is the effect of the zonal gradient of heat exchange.

The angular momentum-based ocean model is capable of representing a single, wind driven gyre. We associate it with the larger, clockwise gyre in the Atlantic basin, south of the gulf stream. Under winter conditions, the centre of this gyre is located at about $30^\circ N$. The maximum of the jet stream intensity is located at about $30^\circ N$ and 10km height. At the earth's surface, however, the maximum intensity of the zonal wind is located at about $40^\circ N$ [Peixoto and Oort, 1992]. Therefore, it drives the ocean gyre in a clockwise direction.

The height dependence of the maximal intensity of the zonal wind is not resolved in the two layer model, nor is the atmospheric boundary layer. Therefore we pose a diagnostic relation to obtain the surface winds from the mean streamfunction, consistent with the observed climatology. As the zonally symmetric pattern, i.e. the jet stream, is equivalent barotropic, we include a scale factor, s , to tune the magnitude of the surface winds. The maximum of the zonal wind is displaced northward by a distance Δ . This yields

$$\bar{U}'_s = -s \frac{\partial}{\partial y'} \bar{\Psi}'(x', y' - \Delta') = \pi s X \cos \pi(y' - \Delta') \quad (11)$$

where U_s is the zonal wind component at 10m height and bars denote zonal averages. This setup is sketched in figure (1). The easterlies along the southern lower boundary of the domain may be thought of as subtropical trade winds. From equation (11) we can calculate the wind stress, τ_1 , which in turn determines the forcing torque T_3 in equation (6). The wind stress is related to the surface winds through

$$\tau_1 = \frac{\rho_a}{\rho_0} C_d U_* \bar{U}_s \quad (12)$$

where ρ_a is the atmospheric density, C_d is the non-dimensional drag coefficient and U_* is the typical (time and zonal average) magnitude of the zonal wind component at the surface.

The forcing due to the wind stress, τ , is given by

$$T_3 = \frac{-1}{V} \iint y \tau_1 dx dy = -\frac{2}{\pi} \frac{\rho_a}{\rho_0} C_d s X U_*' \frac{L}{H} \Sigma_3^2 L^2 \sin \pi \Delta' \quad (13)$$

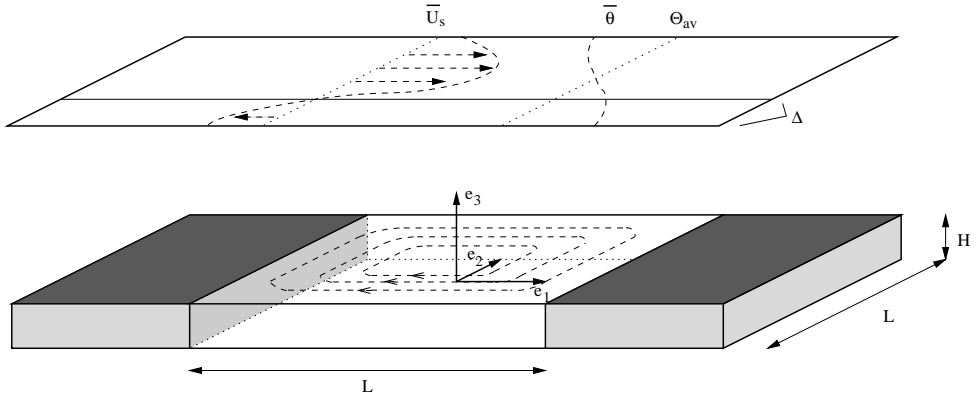


FIGURE 1. Sketch of the geometry of the coupled model. The centre of the jet stream is displaced northward by a distance Δ with respect to the geometrical centre of the ocean basin. Thus, the zonally averaged zonal wind, \bar{U} drives a clockwise circulation in the ocean basin, indicated with dashed lines. Also shown is the profile of $\bar{\theta}$, the zonally averaged departure from the average potential temperature Θ_{av} .

As explained in section (2.1), we need to include a factor of h/H , the relative depth of the mixed layer in the ocean, in the non-dimensional torque T'_3 . The rescaling of \mathbf{u} introduces a factor of $1/2$. This finally results in

$$T'_3 = -\frac{1}{\pi} \frac{\rho_a}{\rho_0} C_{ds} X U_*' \frac{L}{H} \frac{\Sigma_3^2}{\Sigma_1 \Sigma_2} \frac{h}{H} \sin \pi \Delta' \quad (14)$$

The buoyancy forcing consists of a constant part, $F_0^{(y)}$, due to solar heating, and a part due to exchange of sensible heat with the atmosphere, $F_1^{(y)}$. It is given by the surface integral

$$F^{(y)} = \frac{K_v}{V} \iint y \frac{\partial \rho}{\partial z} \Big|_{\frac{H}{2}} dx dy = \frac{\alpha}{V \widehat{\delta \rho} \rho_0 c_p^o} \iint y (-Q + F_{SH}) dx dy = F_0^{(y)} + F_1^{(y)} \quad (15)$$

where c_p^o is the specific heat of the ocean and $\widehat{\delta \rho}$ is the scale of density variations in the mixed layer. The flux of sensible heat, directed out of the ocean, F_{SH} , and the solar heat flux, Q , are in units $[W/m^2]$. We assume that $Q = -y Q_s q / L$, i.e. the solar heating is linear in the latitude with amplitude $Q_s q$, where Q_s is a scale for the meridional gradient in solar heating and q is the non-dimensional forcing strength. This yields

$$F_0^{(y)'} = \frac{1}{12 L \Sigma_1} \frac{L}{H} \frac{\alpha Q_s q}{\widehat{\delta \rho} \rho_0 c_p^o} \quad (16)$$

In terms of the temperature difference between the top of the ocean and the bottom of the atmosphere, F_{SH} is given by

$$F_{SH} = -\rho_a c_p^a C_H U_* (\Theta_s - \Theta^o) \quad (17)$$

where ρ_a is the atmospheric density at the surface and C_H is the dimensionless heat transfer coefficient. For the potential temperature at the 10m level, Θ_s , and the surface potential temperature of the ocean, Θ^o , we substitute

$$\Theta_s = \Theta_{av} + \theta = \Theta_{av} + [\Theta]\tau' \quad (18.1)$$

$$\Theta^o = T_0 - [\Theta^o]\rho(x, y, \frac{H}{2}) = T_0 - [\Theta^o](x\rho_x + y\rho_y + \frac{H}{2}\rho_z) \quad (18.2)$$

where $[\Theta^o] = \widehat{\delta\rho}/\alpha$ is the scale of temperature perturbations in the mixed layer. Using equations (9.2), (18) and (17) we can evaluate the surface integral in equation (15). The result is

$$F_1^{(y)'} = \frac{L}{H} \frac{\rho_a c_p^a}{\rho_0 c_p^o} C_H U_* \left(\frac{2}{\pi^2} \frac{[\Theta]}{[\Theta^o]} X - \frac{1}{12} \rho_y' \right) \quad (19)$$

Note, that we assume a dry atmosphere, and $F_1^{(y)}$ describes sensible heat flux. However, in reality the latent heat flux is larger, of the same order of magnitude as the direct solar forcing. Thus, the flux $F_1^{(y)}$ must be thought of as the sum of sensible and latent heat flux, although there is no explicit evaporation and precipitation in the model.

Finally, there is a feedback term in the atmospheric equations. The forcing term in equation (8.1) consists of a constant part, F_0 , representing the meridional gradient in solar heating, and F_1 , forcing due to heat exchange with the ocean. We assume that the mass in a unit column of air is given by M/L^2 , where $M = p_0 L^2 f / 2g \Sigma_3 \sigma'$ is the mass scale, defined in van Veen [2002]. Thus, the rate of change of the atmospheric temperature due to heat exchange at the ocean's surface is given by $L^2 F_{SH} / c_p^a M$. By the thermal wind relation, (10), this yields a forcing term in the tendency of the shear stream function, τ . The non-dimensional projection onto the zonally symmetric pattern is given by

$$F_1 = - \frac{L^2}{\Sigma_3 [\Theta] c_p^a M} \frac{1}{L^2} \iint F_{SH} \sin \pi y \, dx dy = \frac{L^2 \rho_a C_H U_*}{\Sigma_3 M} \left(\frac{2}{\pi^2} \frac{[\Theta^o]}{[\Theta]} \rho_y' - \frac{1}{2} X \right) \quad (20)$$

In table (1) we have listed all physical constants along with their value in SI units. The scales for length, time, density and temperature have been listed in table (2). With these parameters, the forcing terms (14), (15) and (20) are approximately given by

$$\begin{aligned} T_3' &\approx -X \\ F_1^{(y)'} &\approx 4.6q + 21.7(X - 0.06\rho_y') \\ F_1 &\approx 0.02(0.06\rho_y' - X) \end{aligned} \quad (21)$$

Finally, we redefine the density gradients, dividing them by a factor of $1 + f'^2$. Dropping the primes, the resulting dimensionless equations are

$$\frac{d}{dt_1} \rho_x = -\rho_y L_3 + (\rho_x + f' \rho_y) \rho_z - \rho_x \quad (22.1)$$

$$\frac{d}{dt_1} \rho_y = \rho_x L_3 - (f' \rho_x - \rho_y) \rho_z - \rho_y + k_1 q + k_2 (X - k_3 \rho_y) \quad (22.2)$$

$$\frac{d}{dt_1} \rho_z = -\rho_x^2 - \rho_y^2 - \mu \rho_z \quad (22.3)$$

$$\frac{d}{dt_2} L_3 = -L_3 - k_4 X \quad (22.4)$$

$$\frac{d}{dt_3} X = -Y^2 - Z^2 - aX + aF_0 + \epsilon_1 (k_3 \rho_y - X) \quad (22.5)$$

$$\frac{d}{dt_3} Y = XY - bXZ - Y + G \quad (22.6)$$

$$\frac{d}{dt_3} Z = bXY + XZ - Z \quad (22.7)$$

where $f' = 3.65$, $k_1 = 0.32$, $k_2 = 1.5$, $k_3 = 0.86$, $k_4 = 1$ and $\epsilon_1 = 0.02$. The parameters of the atmosphere model are set to $a = 1/4$, $b = 4$ and $G = 1$. The forcing terms q and F_0 and the coupling strength ϵ_1 will be used as bifurcation parameters.

In equations (22.1-7) we have written derivatives with respect to different time variables. They are related by

$$\frac{d}{dt_3} = \frac{\Sigma_1}{\Sigma_3} \frac{d}{dt_1} \equiv \epsilon_2 \frac{d}{dt_1} \quad \frac{d}{dt_3} = \frac{\Sigma_2}{\Sigma_3} \frac{d}{dt_2} \equiv \epsilon_3 \frac{d}{dt_2} \quad (23)$$

where we have introduced two more small parameters, $\epsilon_{2,3}$, alongside the coupling parameter ϵ_1 . In section (3) an asymptotic analysis will be presented, exploiting the time scale separation and the weak feedback.

System (22) has a feature common for Galerkin truncations of fluid dynamical equations. The linear terms are dissipative, the nonlinear terms are quadratic and conserve the quadratic sum of variables and the forcing terms are constant. A suitable Lyapunov function is given by

$$\mathcal{L} = \rho_x^2 + \rho_y^2 + \rho_z^2 + X^2 + Y^2 + Z^2 \quad (24)$$

A trapping region is then given by

$$\mathcal{L} < \frac{1}{\epsilon_2} (k_1^2 q^2 + F_0^2 + G^2) \equiv R^2 \quad (25)$$

Note, that the vertical angular momentum, L_3 , is not taken into account. This is because the coupling term in equation (22.4) has no counterpart in equation (22.5). This is reasonable because the atmospheric loss of energy due to wind shear forcing is small compared to the heat flux. However, from equation (22.4) it follows that

$$L_3^2 \leq k_4^2 R^2 \quad (26)$$

defines a trapping region for L_3 . Hence, all solutions of system (22) are bounded.

Parameter	Meaning	Value	Unit
L	Length of the basin	$5 \cdot 10^6$	m
H	Depth of the basin	$5 \cdot 10^3$	m
h	Depth of the mixed layer	50	m
f	Coriolis parameter	$7.3 \cdot 10^{-5}$	s^{-1}
g	Acceleration of gravity	10	$m s^{-2}$
α	Thermal expansion coefficient	0.14	$kg m^{-3} K^{-1}$
c_p^a	Specific heat of the dry atmosphere	10^3	$J kg^{-1} K^{-1}$
c_p^o	Specific heat of the ocean	$4.19 \cdot 10^3$	$J kg^{-1} K^{-1}$
p_0	Atmospheric pressure at the surface	10^5	Pa
ρ_a	Atmospheric density at the surface	1.2	$kg m^{-3}$
ρ_o	Reference density in the ocean	10^3	$kg m^{-3}$
r_h	Horizontal Rayleigh damping coefficient	10^{-5}	s^{-1}
r_v	Vertical Rayleigh damping coefficient	$3 \cdot 10^{-8}$	s^{-1}
K_h	Horizontal eddy diffusivity coefficient	10^2	$m^2 s^{-1}$
K_v	Vertical eddy diffusivity coefficient	10^{-4}	$m^2 s^{-1}$
Δ	Displacement of the zonal jet at the surface	10^6	m
C_d	Surface drag coefficient	$1.3 \cdot 10^{-3}$	
C_H	Heat transfer coefficient	$1.3 \cdot 10^{-3}$	
U_*	Typical zonal wind velocity at the surface	10	$m s^{-1}$
Q_s	Meridional difference in solar heating	200	$W m^{-2}$
s	Vertical scale factor of the zonal wind	0.2	
σ	Static stability of the atmosphere	22	K

TABLE 1. Parameters in the coupled model. Numerical values taken from Maas [1994], van der Schrier and Maas [1998] and Peixoto and Oort [1992]. Note, that r_h has been chosen large in order to yield a realistic density scale. In van der Schrier and Maas [1998] r_h is smaller, but the scaling factor $1 + f'^2$ is of order 10^3 , so that a comparable effective density scale is used.

3. Asymptotic analysis with a passive atmosphere

As we have seen, the weak feedback to the atmosphere and the difference in time scales introduce small parameters in the coupled model. For simplicity, we scale them with a single small parameter:

$$\epsilon_1 = 2 \cdot 10^{-2} = O(\epsilon) \quad \epsilon_2 = 3 \cdot 10^{-5} = O(\epsilon^2) \quad \epsilon_3 = 2 \cdot 10^{-2} = O(\epsilon) \quad (27)$$

System (22) can then be written as

$$\begin{aligned} \frac{d}{dt_1} \mathbf{Y} &= \mathbf{g}(\mathbf{Y}, L_3, \mathbf{X}_1) \\ \epsilon \frac{d}{dt_1} L_3 &= -L_3 - k_4 \mathbf{X}_1 \\ \epsilon^2 \frac{d}{dt_1} \mathbf{X} &= \mathbf{f}_0(\mathbf{X}) + \epsilon \mathbf{f}_1(\mathbf{X}_1, \mathbf{Y}_2) \end{aligned} \quad (28)$$

Length			
	horizontal	L	$5 \cdot 10^3 \text{ km}$
	vertical	H	5 km
Time			
	overturning	$\Sigma_1^{-1} = L^2/12K_h$	500 years
	wind driven	$\Sigma_2^{-1} = r_v^{-1}$	1 year
	atmospheric	Σ_3^{-1}	7 days
Density variations			
	interior	$[\hat{\delta}\rho] = 12\rho_0 r_h K_h / gH$	$2.4 \cdot 10^{-4} \text{ kg m}^{-3}$
	mixed layer	$[\hat{\delta}\rho] = \alpha Q_s f L^2 / \rho_0 g c_p^o h^2$	0.5 kg m^{-3}
Temperature			
	atmosphere	$[\Theta] = f \Sigma_3 L^2 / d c_p$	24 K
	mixed layer	$[\Theta^o] = \hat{\delta}\rho / \alpha$	3.6 K
Mass			
	atmosphere	$M = p_0 L^2 f [\Theta] / 2g \Sigma_3 \sigma$	$7.7 \cdot 10^{18} \text{ kg}$

TABLE 2. Scales for the ocean and the atmosphere model. The atmospheric time scale is the damping time scale of baroclinic waves due to Hamiltonian cooling and interlayer friction, see van Veen [2002]. In the right column the order of magnitude.

where we have introduced $\mathbf{Y} = (\rho_x, \rho_y, \rho_z)^T$ and $\mathbf{X} = (X, Y, Z)^T$. As a consequence of Fenichel's theorem [Wiggins, 1994], hyperbolic equilibria of the system with $\epsilon = 0$ give a first approximation of a slow manifold in the system with nonzero ϵ . In order to asymptotically approximate the dynamics on the slow manifold, we substitute the regular expansion

$$L_3 = L_3^{(0)} + \epsilon L_3^{(1)} + \dots \quad \mathbf{X} = \mathbf{X}^{(0)} + \epsilon \mathbf{X}^{(1)} + \dots \quad (29)$$

In the limit $\epsilon \downarrow 0$ we find

$$\mathbf{f}_0(\mathbf{X}^{(0)}; F_0) = 0 \quad (30)$$

Thus, a three dimensional slow manifold of equations (28) is approximated by the equilibria of the uncoupled Lorenz model. The solutions of equation (30), and their linear stability, can be found explicitly as the roots of a third order polynomial equation [Sicardi and Masoller, 1996; Shilnikov et al., 1995]. In figure (2) the branch of equilibria is shown. Two saddle node bifurcations occur, so that there is one equilibrium or there are three. The Hopf bifurcation, labeled HB, represents the baroclinic instability in the Lorenz model. Away from the saddle node bifurcations, \mathbf{f}_0 can locally be inverted so that we can write $\mathbf{X}^{(0)} = \phi(F_0)$, with $\mathbf{f}_0(\phi; F_0) = 0$. On the intermediary time scale $L_3^{(0)}$ relaxes towards an equilibrium with $\mathbf{X}^{(0)}$, given by

$$L_3^{(0)} = -k_4 \mathbf{X}_1^{(0)} \quad (31)$$

Together, equations (30) and (31) approximate an extended, four dimensional slow manifold of the coupled system.

The slow dynamics is described by $\dot{\mathbf{Y}} = \mathbf{g}(\mathbf{Y}, -k_4\phi_1, \phi_1)$. A familiar form of these equations is obtained if we first shift $\mathbf{Y}_3 \rightarrow \bar{\mathbf{Y}}_3 = \mathbf{Y}_3 + k_4\phi_1/f'$ and subsequently scale time and \mathbf{Y} by a factor $1 + k_4\phi_1/f'$. This yields

$$\frac{d}{dt_1} \mathbf{Y}_1 = -\mathbf{Y}_1 + \mathbf{Y}_1 \bar{\mathbf{Y}}_3 + B \mathbf{Y}_2 \bar{\mathbf{Y}}_3 \quad (32.1)$$

$$\frac{d}{dt_1} \mathbf{Y}_2 = -\mathbf{Y}_2 + \mathbf{Y}_2 \bar{\mathbf{Y}}_3 - B \mathbf{Y}_1 \bar{\mathbf{Y}}_3 + \mathcal{G} - C \mathbf{Y}_2 \quad (32.2)$$

$$\frac{d}{dt_1} \bar{\mathbf{Y}}_3 = -\mathbf{Y}_1^2 - \mathbf{Y}_2^2 - A \bar{\mathbf{Y}}_3 + A \mathcal{F} \quad (32.3)$$

Apart from the extra damping term in equation (32.2), these are the equations of the Lorenz model (8), with parameters depending on ϕ according to

$$\begin{aligned} A &= \frac{f' \mu}{f' + k_4 \phi_1} & C &= \frac{f' k_2 k_3}{f' + k_4 \phi_1} & \mathcal{G} &= \frac{f' k_1 q + f' k_2 \phi_1}{f' + k_4 \phi_1} \\ B &= f' & \mathcal{F} &= \frac{k_4 \phi_1}{f'} \end{aligned} \quad (33)$$

The similarity between the ocean model and the Lorenz model was already pointed out in Maas [1994]. There, the choice of parameters guaranteed that no complex behaviour occurred. Here, this is not clear from the outset as we have an extra damping term and forcing that depends on the atmospheric parameters through ϕ_1 . Because of the extra damping term we cannot exactly solve for the equilibria of system (32), as this involves finding roots of a fifth order polynomial equation. We can, however, check numerically what kind of dynamics arise as we vary F_0 , thereby altering the atmosphere's equilibrium state, ϕ . Continuation, by means of software package AUTO [Doedel et al., 1986], indicates that a stable equilibrium state is the unique limit set of system (32) for $0 < F_0 < 100$ and $q = 1$. This equilibrium state corresponds to a statically stable state of the ocean, i.e. $\rho_z < 0$.

The first order terms are given by

$$L_3^{(1)} + k_4 \mathbf{X}_1^{(1)} = 0 \quad \mathbf{X}^{(1)} = -D\mathbf{f}_0^{-1} \mathbf{f}_1(\phi_1, \mathbf{Y}_2) \quad (34)$$

Here, the inverse of the Jacobian matrix at ϕ enters the equations. As long as $\mathbf{X}^{(1)}$ is of order one, the dynamically and statically stable equilibrium state of the ocean model, found in the lowest order approximation, will persist. If, however, F_0 is chosen near a saddle node bifurcation of the atmospheric equilibrium, $D\mathbf{f}_0$ becomes nearly singular and the ocean's equilibrium state might bifurcate. In this situation the feedback loop in system (22), otherwise weak because of the small parameter ϵ_1 , becomes strong due to the sensitive dependence of the atmosphere's equilibrium state on the feedback, \mathbf{f}_1 .

Thus, GSP analysis shows that we have four possibilities for the behaviour of the coupled model, depending on the equilibria of the Lorenz-84 model, labeled 1 to 4 in figure (2):

- (1) There is one stable equilibrium. This equilibrium corresponds to a stable slow manifold in the coupled system. The dynamics on this slow manifold consists of a relaxation towards a statically stable equilibrium state in the ocean model.

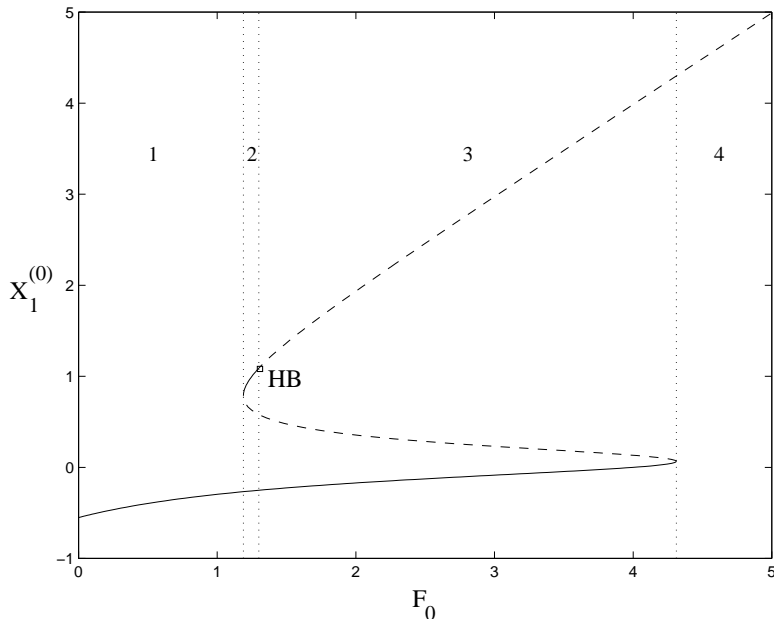


FIGURE 2. Continuation of the equilibria of the Lorenz-84 model for $G = 1$. The numbers 1 to 4 denote the different cases listed in section 3. Solid branches are stable and dashed branches are unstable.

- (2) There are three equilibria, one is of saddle type whereas the other two are stable. Each of these equilibria corresponds to a slow manifold in the coupled system, two of which are stable. The dynamics on a slow manifold consists of a relaxation towards a statically stable equilibrium state in the ocean model. Only if the corresponding atmospheric equilibrium is nearly critical, the ocean model's equilibrium can bifurcate and periodic oscillations can occur on the slowest time scale. This situation is described in section (4.1).
- (3) There are three equilibria, one of which is stable whereas the other two are of saddle type. This situation occurs beyond Hopf bifurcation HB, where a stable cycle is produced. Depending on the initial conditions, the coupled system can either settle on the slow manifold corresponding to the stable equilibrium or be attracted to the stable cycle on the fast time scale. As shown in section (4), no bifurcations of the ocean model's equilibrium occur on the stable slow manifold.
- (4) There is one equilibrium of saddle type. The corresponding slow manifold is unstable and the coupled system is attracted to the stable cycle on the fast time scale. For higher values of F_0 , this cycle bifurcates and more complex behaviour sets in, as shown in section (4.2).

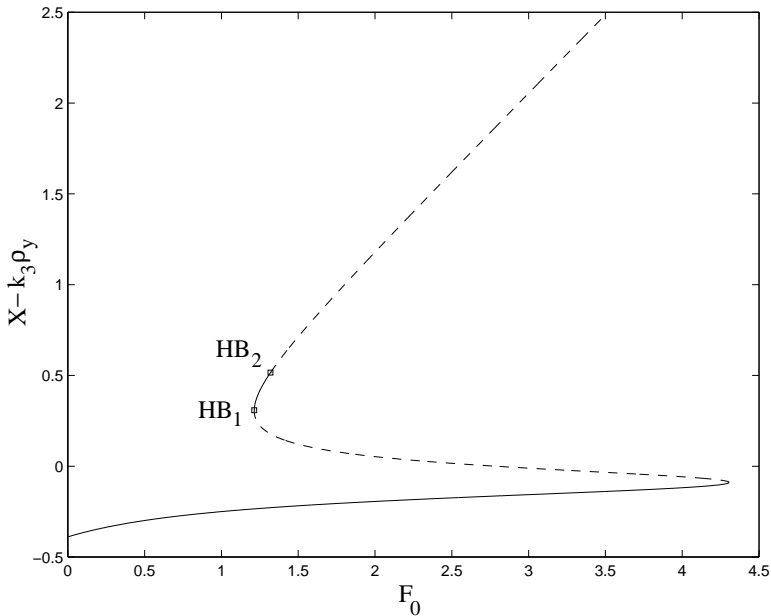


FIGURE 3. Continuation of the equilibrium state of the Lorenz-Maas model. Solid lines represent stable branches, dashed lines represent unstable branches. Hopf bifurcations have been labeled $HB_{1,2}$.

4. Bifurcation analysis of the coupled system

In figure (3) the branch of equilibria of the coupled system (22) is shown. We have fixed $q = 1$ and $\epsilon_1 = 0.02$ and increased F_0 from zero. On the vertical axis we have plotted the meridional gradient of the heat flux at the ocean's surface. In the lower, stable, branch of equilibria this flux strengthens the zonal jet in the atmosphere, i.e. $F_1 > 0$. In the upper branch it weakens the zonal jet, i.e. $F_1 < 0$. The latter situation agrees with the annual mean distribution of sensible heat flux at the surface [Peixoto and Oort, 1992, chapter 10].

The first Hopf bifurcation, labeled HB_1 , occurs near a saddle node bifurcation and is not present in the uncoupled Lorenz model. It corresponds to case 2 discussed in section (3). Here, an unstable cycle with a period of order one in units Σ_1^{-1} is created. In section (4.1) it is shown that the presence of this Hopf bifurcation near the saddle node bifurcation is connected to a Bogdanov-Takens point, at which the equilibrium has two zero eigenvalues.

The rightmost Hopf bifurcation, labeled HB_2 , represents the atmosphere model's baroclinic instability. It produces a cycle with a period of order one in units Σ_3^{-1} , which represents a traveling baroclinic wave. If the forcing is increased this cycle bifurcates and complex behaviour arises. The route to chaos through bifurcations of the cycle and intermittent behaviour are described in sections (4.2) and (4.2), respectively.

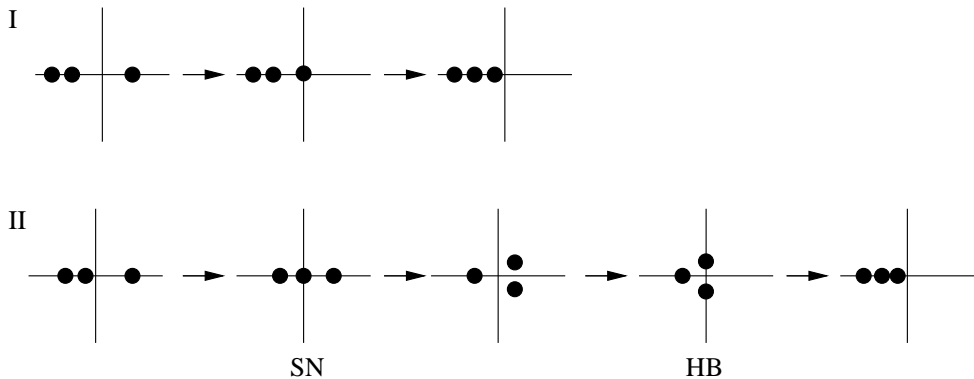


FIGURE 4. Bifurcation scenario along the branch of equilibria of the Lorenz model (I) and the Lorenz-Maas model (II): eigenvalues in the complex plane. The saddle node (fold) bifurcation has been labeled SN and the Hopf bifurcation HB . In scenario II only the leading eigenvalues are shown. Compare to figures (2) and (3).

4.1. The Bogdanov-Takens singularity. At Hopf bifurcation HB_1 a cycle is created with a period of about 500 years, the overturning time scale Σ_1^{-1} . The behaviour of the eigenvalues along the branch of equilibria, shown in figure (3), is portrayed in figure (4). The periodic orbit exists to the right of HB_1 and has one unstable multiplier. If F_0 is increased slightly, it becomes homoclinic to the saddle type equilibrium. This can be understood from the unfolding of the Bogdanov-Takens singularity which occurs if the fold and Hopf bifurcations in scenario II coincide. The unfolding of this singularity is described in Kuznetsov [1998], chapter 8. As predicted by the asymptotic analysis of section (3), the distance between the bifurcation points in parameter space is rather small, about $2 \cdot 10^{-5}$ and thus of the order of ϵ_2 . The clearest picture is obtained by unfolding the codimension two singularity in parameters q and ϵ_1 , i.e. the solar forcing in the ocean model and one coupling parameter, as shown in figure (5). When increasing ϵ_1 from zero, at first there is no Hopf bifurcation. Scenario I is followed when we continue the equilibrium in parameter q . At the critical value of ϵ_1 a pair of zero eigenvalues appears. This is the codimension two Bogdanov-Takens point. At this point a Hopf curve and a homoclinic bifurcation curve originate. If we increase ϵ_1 further, scenario II is followed.

Along the homoclinic bifurcation line, the saddle value, i.e. the sum of the unstable eigenvalue and the (real part of the) leading stable eigenvalue, is small ($\lesssim 10^{-2}$) but positive. Therefore, the homoclinic connection and the periodic orbit that connects to the Hopf line are weakly unstable. In figure (6) the homoclinic connection is shown, along with an 50.000 year integration, started near the saddle type equilibrium. On the long time scale, Σ_3^{-1} , the system relaxes towards the stable focus on the upper branch in diagram (3), with the realistic surface flux. In terms of phase relations between the density gradients $\rho_{x,y,z}$, this damped oscillation is similar to the oscillatory cycle found in the uncoupled Maas model [Maas, 1994]. In

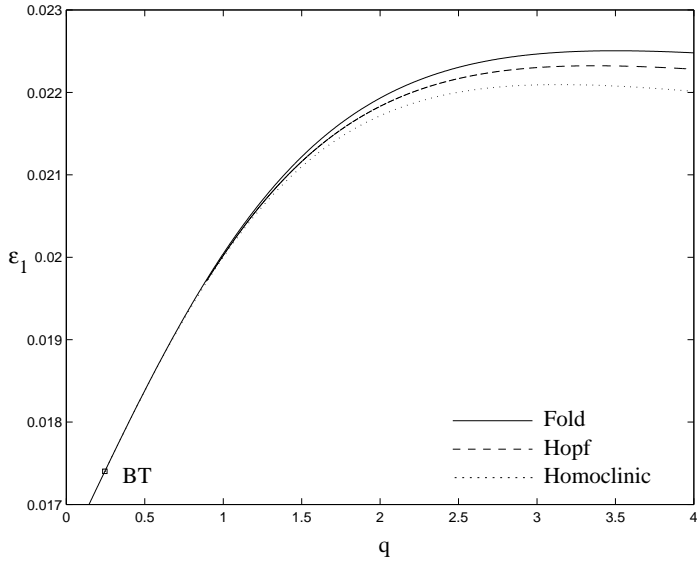


FIGURE 5. Unfolding of the Bogdanov-Takens singularity in q and ϵ_1 , for $F_0 = 1.21374$. On the Hopf line an unstable periodic orbit is created which becomes homoclinic to the saddle type equilibrium, i.e. the middle branch in figure (3).

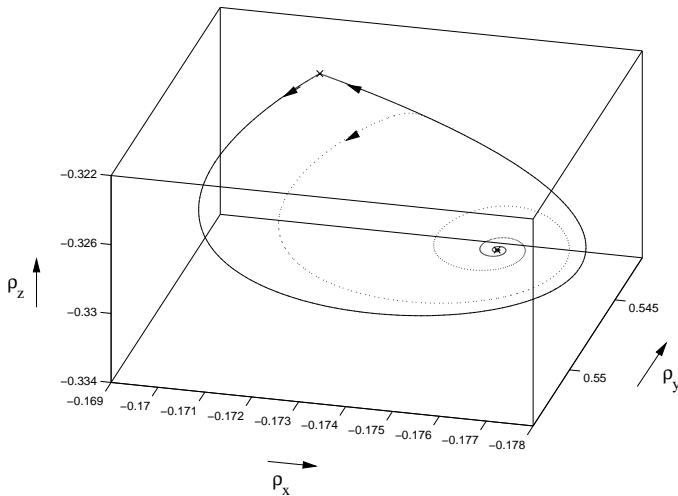


FIGURE 6. Damped oscillation on the time scale Σ_1^{-1} , for $\epsilon_1 = 0.0217$ and $q = 2$. The solid line is the homoclinic connection, the dashed line is forward integration. The saddle, in the top left corner, and the stable focus, in the bottom right corner, have been marked with crosses. The integration time was $\Delta t_1 = 100$.

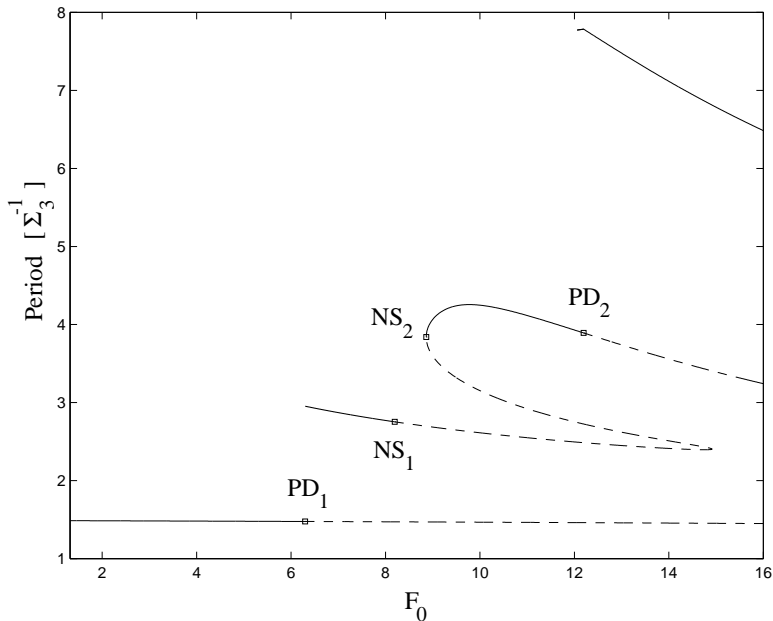


FIGURE 7. Continuation of the cycle produced at HB_2 . Solid lines denote stable branches, dashed lines denote unstable branches. Period doubling bifurcations have been marked $PD_{1,2}$ and Neimark-Sacker bifurcations $NS_{1,2}$. For values of F_0 between bifurcation points NS_1 and NS_2 the behaviour is chaotic, periodic with high period ($O(10) [\Sigma_3^{-1}]$) or intermittent.

one phase of the oscillation the meridional density gradient, ρ_y is relatively low, and the zonal density gradient, ρ_x , relaxes due to friction and dissipation. The overturning circulation weakens. In the second phase, the differential solar heating builds up the meridional density gradient, which strengthens the overturning through the geostrophic coupling to ρ_x . The overturning circulation then weakens the meridional gradient and the cycle is closed. It might be expected that this cycle can not occur if the coupling through the vertical angular momentum, L_3 , is strong. In that case, the horizontal components of the density gradient will be mixed and the interplay between the damped overturning circulation and the forcing due to meridional differential heating will be destroyed. Indeed, if k_4 is increased to about 1.5, the Hopf bifurcation HB_1 disappears. As prescribed by GSP theory, discussed in section (3), the fast, atmospheric, variables are slaved during the oscillation, in instantaneous balance with the feedback term \mathbf{f}_1 .

4.2. Bifurcations of limit cycles and chaos. In diagram (7), the continuation of the cycle, originating at HB_2 , is shown. Initially it is stable. At the first period doubling bifurcation, labeled PD_1 , a stable cycle of twice the period is created. This cycle becomes unstable through a Neimark-Sacker bifurcation, labeled NS_1 . The period doublings $PD_{1,2}$ and Neimark-Sacker bifurcation NS_1 are also

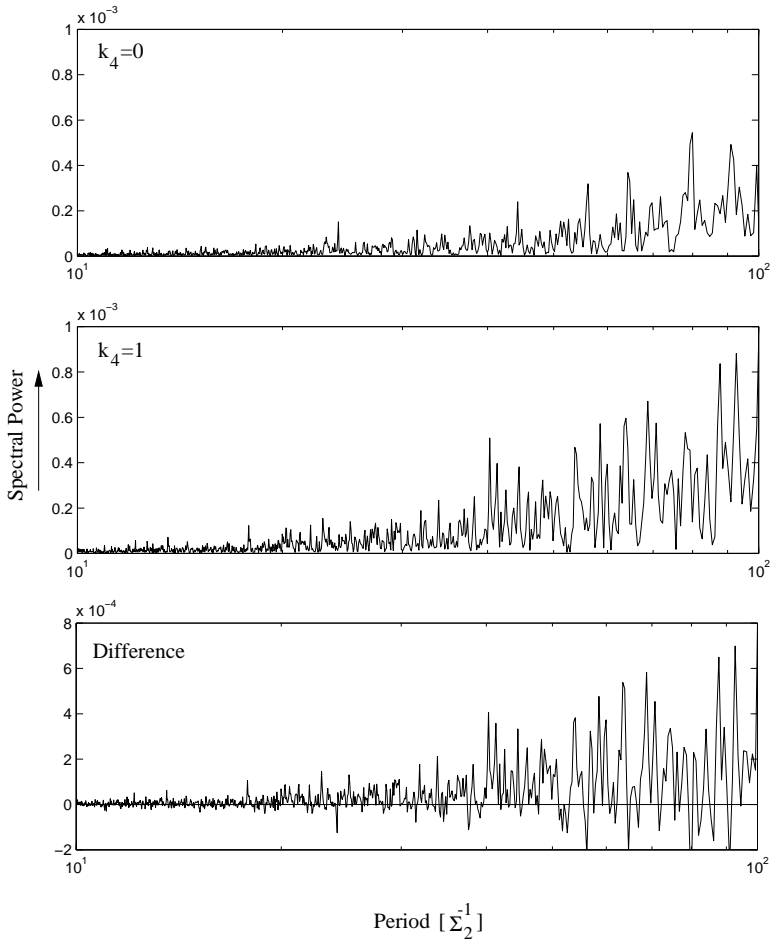


FIGURE 8. Power spectra of ρ_y from a 15,000 year integration in the chaotic regime with $F_0 = 8.25$. Top: $k_4 = 0$, middle: $k_4 = 1$, bottom: difference. Note, that the vertical scales are almost the same. The horizontal scale is logarithmic, spanning $10 - 100 [\Sigma_2^{-1}] \approx 10 - 100 \text{ yrs}$.

present in the uncoupled Lorenz model [Shilnikov et al., 1995]. In van Veen [2002] it was shown that beyond NS_1 a sudden transition to chaos occurs following the Ruelle-Takens scenario [Ruelle and Takens, 1971]. This also happens in the coupled model. The behaviour becomes chaotic, with tiny periodic intervals in parameter space. This behaviour is similar to that of the Lorenz-Stommel model, as described in Roebber [1995]; van Veen et al. [2001]. In the chaotic regime, there is very little variability in the slow subsystem. Therefore, it can be characterised as a regime with a passive ocean.

The regime with a chaotic atmosphere and a passive ocean can be regarded as the model's representation of the real climate. Therefore, we list a number of average

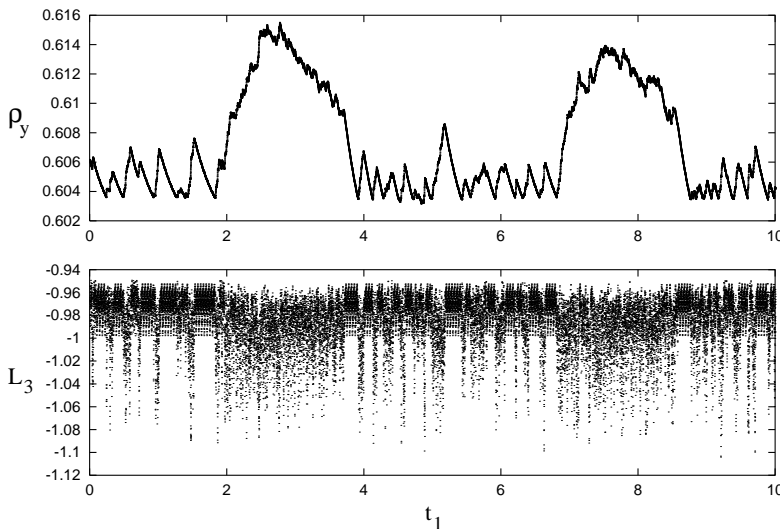


FIGURE 9. Intermittency in the Lorenz-Maas model. The meridional density gradient, ρ_y , and the vertical angular momentum, L_3 , against t_1 .

physical quantities to validate the model. The average values were obtained from a 15.000 year integration at $F_0 = 8.25$. The vertical mean intensity of the zonal jet is about 26 ms^{-1} , which yields a maximal zonal wind at the surface of about 5.2 ms^{-1} with an associated surface wind stress of about 8.1 Pa . The meridional density difference in the ocean's mixed layer is about 4.3 kgm^{-3} , corresponding to a difference in sea surface temperature of about 30 K . The meridional difference in heat flux into the atmosphere is about 260 W . Finally, a measure for the overturning circulation is given by $\sqrt{L_1^2 + L_2^2} \approx 1.1 \cdot 10^4 \text{ m}^2 \text{ s}^{-1}$. These values agree reasonably well with climatological means [Peixoto and Oort, 1992], although the zonal jet intensity and the sea surface temperature difference are exaggerated by a factor of about 1.2. Considering the few degrees of freedom of the coupled model it reproduces the climatological values well.

The deviation from the mean value of the meridional sea surface temperature difference is slightly underestimated: typically about 0.2 K compared to a measured standard deviation induced by synoptic-scale eddies of 0.5 K . The deviation from the mean value of the vertical mean zonal jet intensity agrees with the measured value of about 8 ms^{-1} .

In order to investigate the influence of the coupling through the wind driven circulation in this regime, we produced power spectra of a 15.000 year integration with $k_4 = 1$ and $k_4 = 0$, shown in figure (8). In the latter case only the coupling through heat exchange remains. As L_3 forces the density gradients through advection, we expect to see an increase in the spectral power of ρ_y on a decadal time scale if the coupling is switched on. This is best visible in the bottom picture, the difference of the spectra with and without wind driven circulation. The difference is of the same order of magnitude as the power in the individual spectra.

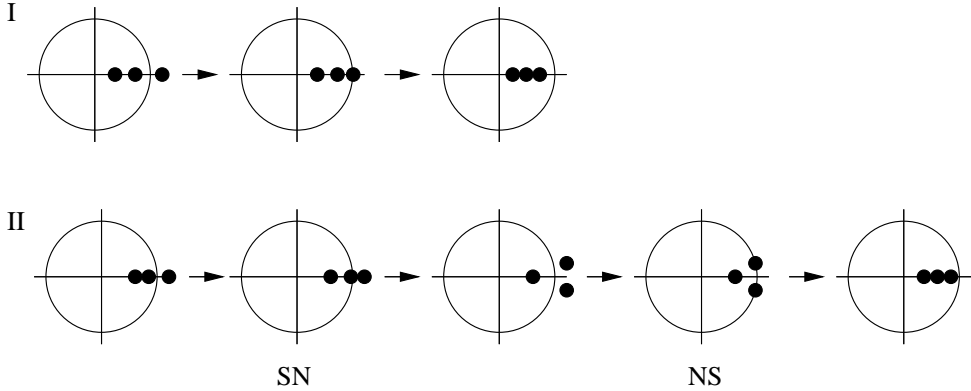


FIGURE 10. Bifurcation scenario along a branch of periodic solutions of the Lorenz-84 model (I) and the Lorenz-Maas model (II): Floquet multipliers in the complex plane. The saddle node (fold) bifurcation has been labeled SN and the Neimark-Sacker bifurcation *NS*. In scenario II only the leading multipliers are shown.

4.3. Ocean-atmosphere interaction through intermittency. The ocean plays an active role near the boundaries of the periodic intervals, where intermittency can occur. Ample discussion of this behaviour was given in van Veen et al. [2001]. In figure (9) we show an intermittent time series of the Lorenz-Maas model, obtained from a 5.000 year integration. As in the Lorenz-Stommel model, the intermittency is of type II in terms of the classification by Pomeau and Manneville [1980], meaning that the periodic orbit involved loses its stability through a Neimark-Sacker bifurcation. In the coupled model, Neimark-Sacker bifurcations tend to occur close to fold bifurcations. This scenario is illustrated in figure (10). In the uncoupled Lorenz model, scenario I, a single, real Floquet multiplier crosses the unit circle. In the coupled model, scenario II, a real multiplier crosses the unit circle in the opposite direction and forms a complex pair with the unstable multiplier. The complex pair crosses back into the unit circle, causing a Neimark-Sacker bifurcation. The distance in parameter space between the fold and the Neimark-Sacker bifurcations is typically of the same order of magnitude as the ratio of time scales $\epsilon_2 = \Sigma_3/\Sigma_1 \approx 10^{-5}$. This scenario is also followed around bifurcation point NS_2 , on the second branch of periodic orbits in figure (7). The long time scale, Σ_1^{-1} , shows up in the intermittent dynamics because the rate of convergence to, and departure from the saddle type periodic orbit is set by the leading multipliers, two of which are associated with the slow subsystem.

The bifurcation scenarios for periodic orbits, shown in figure (10), are analogous to those of equilibria, discussed in section (4.1). Again, the ocean can play an active role in the coupled dynamics near a bifurcation point of the model.

5. Conclusion

We have presented a low-order ocean-atmosphere model which combines wind driven and overturning circulation. The coupling terms, both through wind torque forcing and heat exchange at the interface, have been derived from the boundary conditions of the ocean model. The model describes the clockwise gyre, south of the gulf stream in the North Atlantic, coupled to a midlatitude, geostrophic atmosphere with baroclinic waves.

Due to the difference in time scales of wind driven, overturning and atmospheric dynamics, as well as to the weak feedback to the atmosphere, small parameters appear in the model. By means of GSP theory, the coupled model is reduced to an approximate slow manifold. Analysis of the reduced dynamics shows that, as long as the atmospheric equilibrium is not near a saddle-node bifurcation, only relaxation towards a dynamically and statically stable equilibrium can occur in the ocean model. If the atmospheric equilibrium becomes nearly critical, a Hopf instability can be induced in the slow dynamics.

At this Hopf bifurcation a cycle, with a period on the overturning time scale, is created. A bifurcation analysis in two parameters leads to a Bogdanov-Takens point, where the saddle-node and the Hopf bifurcations coincide. The unfolding of this codimension two point shows, that the Hopf bifurcation disappears if the feedback parameter is smaller than a critical value and if the coupling through wind driven circulation is stronger than a critical value. It also shows, that the cycle, created at the Hopf bifurcation, becomes homoclinic if the forcing is increased slightly. The homoclinic connection is weakly unstable, and integrations show damped oscillations towards a stable equilibrium on the slow (overturning) time scale. During these oscillations the atmospheric variables are passive, in instantaneous balance with the ocean's feedback.

If the solar forcing parameter in the atmosphere model is increased, its equilibrium state becomes unstable through a Hopf bifurcation which represents the baroclinic instability. A stable cycle is created with a period of the order of one week. The continuation of this cycle to higher values of the solar forcing shows that, in a window in parameter space, chaotic behaviour arises. Some averaged physical quantities, obtained from a forward integration in the chaotic regime, are compared to their observed climatological means. In spite of its simplicity, the coupled model reproduces the observed values well. The intensity of the zonal jet in the atmosphere and the meridional sea surface temperature difference are slightly exaggerated. A comparison of power spectra with and without wind driven circulation reveals that the coupling through wind stress forcing adds to the energy in decadal modes of the ocean's variables.

Typically, tiny windows of periodicity exist amidst the chaos. Near the boundary of stability of such windows, intermittency is observed. This situation is very similar to the one found in van Veen [2002]. In the fully chaotic regime, the ocean can be considered passive. The slow variables have very small amplitude and merely integrate the atmospheric forcing. During the intermittent behaviour, the ocean

plays an active role, as it repeatedly pushes the atmosphere through the boundary of periodic and chaotic behaviour.

The low-order climate model presented here can readily be extended to include more physics and more detail. In contrast to, e.g. Nakamura et al. [1994] and van Veen [2002], both constituents of the model are scalable, i.e. based on Galerkin truncation. Extensions of the model, to be studied in future research, include:

- Taking into account salinity in the ocean model, after van der Schrier and Maas [1998], allowing for a study of the full thermohaline circulation. A parameterisation of water vapour transport in the atmosphere then has to be designed. Thus, the effect of the meridional profile of precipitation can be studied. Also, the ocean model with salinity can display chaotic behaviour and thus play a more active role in the coupled dynamics.
- Adding more modes to the atmosphere model, allowing for more complex internal atmosphere dynamics such as vacillation [De Swart, 1989]. The internal dynamics of the atmosphere then includes a wider range of time scales, overlapping with the time scale of wind driven circulation.
- Adding more modes to the ocean model in order to extend it to a double gyre or two hemispheres. Inclusion of nonlinear modes is, however, not straightforward in view of the treatment of the pressure torque [Maas, 2002].
- Explicitly representing the ocean's mixed layer such as to avoid some of the parameterisations in section (2.2). This may lead to a better description of the coupling between wind driven and overturning circulation through advection of sea surface temperature anomalies.

Thus, a family of low-order models is set up which allows for the mathematical analysis of important feedback loops in the climate system.

6. Acknowledgments

The author would like to thank Ferdinand Verhulst, Theo Opsteegh, Leo Maas, Gerard van der Schrier, Frank Selten and Reindert Haarsma for useful discussions and proofreading. This work is part of the NWO project 'a conceptual approach to climate variability' (nr. 61-620-367).

Bibliography

- Arnold, L. & Olbers, D. [2002] Private communications.
- De Swart, H. E. [1989] “Analysis of a six-component atmospheric spectral model: chaos, predictability and vacillation,” *Physica D* **36**, 222–234.
- Doedel, E., Champneys, A., Fairgrieve, T., Kuznetsov, Yu. A., Sandstede, B. & Wang, X.J. [1986] *AUTO97: Continuation and bifurcation software for ordinary differential equations (with HomCont)* Computer Science, Concordia University, Montreal, Canada.
- Huang, R. X. & Stommel, H. M. [1992] “Convective flow patterns in an eight-box cube driven by combined windstress, thermal and saline forcing,” *J. Geophys. Res.* **97**, 2347–2364.
- Ierley, G. R. & Sheremet, V. A. [1995] “Multiple solutions and advection-dominated flows in the wind-driven circulation. part I: Slip,” *J. Mar. Res.* **53**, 703–737.
- Kuznetsov, Yu. A. [1998] *Elements of applied bifurcation theory* (Springer, New York).
- Lorenz, E. N. [1984] “Irregularity: a fundamental property of the atmosphere,” *Tellus* **36A**, 98–110.
- Maas, L. R. M. [1994] “A simple model for the three-dimensional, thermally and wind-driven ocean circulation,” *Tellus* **46A**, 671–680.
- Maas, L. R. M. [2002] “Basin scale dynamics of a stratified rotating fluid,” In preparation.
- Monahan, A. H. [2001] “Lyapunov exponents of a simple stochastic model of the thermally and wind-driven ocean circulation,” Submitted to *Dyn. Atmos. Ocean.*
- Nakamura, M., Stone, P. H. & Marotzke, J. [1994] “Destabilization of the thermohaline circulation by atmospheric eddy transports,” *Journal of Climate* **7**, 1870–1882.
- Peixoto, J.P. & Oort, A.H. [1992] *Physics of climate* (American Institute of Physics).
- Pomeau, Y. & Manneville, P. [1980] “Intermittent transition to turbulence in dissipative dynamical systems,” *Commun. Math. Phys.* **74**, 189–197.
- Rödenbeck, C., Beck, C. & Kantz, H. “Dynamical systems with time scale separation: averaging, stochastic modelling and central limit theorems,” In Imkeller, P. & von Storch, J. S., editors, *Stochastic climate models*. Birkhauser, [2001].
- Roebber, P. J. [1995] “Climate variability in a low-order coupled atmosphere-ocean model,” *Tellus* **47A**, 473–494.
- Ruelle, D. & Takens, F. [1971] “On the nature of turbulence,” *Commun. math. Phys.* **20**, 167–192.

- Shilnikov, A., Nicolis, G. & Nicolis, C. [1995] “Bifurcation and predictability analysis of a low-order atmospheric circulation model,” *Internat. J. Bifur. Chaos* **5(6)**, 1701–1711.
- Sicardi, A. C. & Masoller, C. [1996] “Analytical study of the codimension two bifurcation of the new Lorenz system,” *Instabilities and Nonequilibrium Structures V*, 345–348.
- Stommel, H. [1961] “Thermohaline convection with two stable regimes of flow,” *Tellus* **13**, 224–230.
- Titz, S., Kuhlbrodt, T., Rahmstorf, S. & Feudel, U. [2002] “On freshwater-dependent bifurcations in box models of the interhemisphere thermohaline circulation,” *Tellus* **54A**, 89–98.
- Schrier, G. van der & Maas, L. R. M. [1998] “Chaos in a simple model of the three-dimensional salt-dominated ocean circulation,” *Climate Dynamics* **14**, 489–502.
- Veen, L. van [2002] “Baroclinic flow and the Lorenz-84 model,” *Internat. J. Bifur. Chaos*. To appear (chapter 2 of this thesis).
- Veen, L. van , Opsteegh, T. & Verhulst, F. [2001] “Active and passive ocean regimes in a low-order climate model,” *Tellus* **53A**, 616–627 (chapter 3 of this thesis).
- Veronis, G. [1963] “An analysis of wind-driven ocean circulation with a limited number of Fourier components,” *J. Atmos. Sci.* **20**, 577–593.
- Welander, P. [1982] “A simple heat-salt oscillator,” *Dyn. Atmos. Ocean.* **6**, 233–242.
- Wiggins, S. [1994] *Normally hyperbolic invariant manifolds in dynamical systems* (Springer Verlag).